frontiers in Earth Science

TYPE Original Research
PUBLISHED 23 March 2026
DOI 10.3389/feart.2026.1781404

OPEN ACCESS

EDITED BY
Matteo Del Soldato,
University of Florence, Italy

REVIEWED BY
Matteo Fiorucci,
University of Cassino, Italy
Filippo Vecchiotti,
Central Institution for Meteorology and Geodynamics (ZAMG), Austria

*CORRESPONDENCE
Massimo Fabris,
massimo.fabris@unipd.it

RECEIVED 05 January 2026
REVISED 26 February 2026
ACCEPTED 27 February 2026
PUBLISHED 23 March 2026

CITATION
Fabris M and Nazari S (2026) Analysis of InSAR datasets from the EGMS and Veneto region using ground-based GNSS velocities for the monitoring of land subsidence in the Po river delta (Italy).
Front. Earth Sci. 14:1781404.
doi: 10.3389/feart.2026.1781404

Analysis of InSAR datasets from the EGMS and Veneto region using ground-based GNSS velocities for the monitoring of land subsidence in the Po river delta (Italy)

Massimo Fabris[1]* and Shokrullah Nazari[2]

[1]Department of Civil, Environmental and Architectural Engineering, University of Padua, Padua, Italy, [2]Independent Researcher, Padua, Italy

Global navigation satellite system (GNSS) and interferometric synthetic aperture radar (InSAR) are used in the monitoring of structures, infrastructures and ground deformations. In many cases satellite data are calibrated and validated using ground-based information. In this context, the increasing number of sensors, fixed on structures or mounted on satellites, that permanently and automatically acquire information, are generating large open datasets used by many researchers in many different fields and for many different applications. Calibration, validation, and evaluation of the performance and quality of these large datasets will pose a real challenge in the coming years. An example is given by the open InSAR data available from the European ground motion service (EGMS) of the Copernicus program and Veneto Region databases. Few information about the quality of these datasets are often available: not always the data are checked, calibrated, and validated; they may contain outliers, biases, unquantified uncertainties, etc. In this work, interferometric information available from the EGMS dataset (ascending tracks 44 and 117, and descending track 95), and Veneto Region dataset (ascending track 117 and descending track 95), were calibrated and validated using ground-based GNSS data from 3 continuous stations and 46 non-permanent sites (NPS) of the Po delta network (PODELNET); subsequently, the data were integrated to monitor land subsidence in the Po river delta (PRD), located in northern Italy. In this way, this study gave an opportunity to analyse open InSAR datasets by means of reference ground-based information during the period 2018–2022. This is the first study to systematically validate EGMS and Veneto Region InSAR data against a dense GNSS network in the PRD. The results allowed to verify that in the study area the EGMS data do not require a calibration, while for the Veneto Region InSAR velocities the calibration is recommended. The integration of GNSS and InSAR data allowed to extract maps of land subsidence in an integrated monitoring system. The velocities obtained showed increasing values from west to east in the PRD; the maximum values, up to –15 mm/year, were detected along the coastal area, where sea embankments

are exposed to increasing risks of instability exacerbated by the rise of sea level caused by climate change.

KEYWORDS

Calibration, Comparison, GNSS observations, InSAR datasets, land subsidence, po river Delta, validation

1 Introduction

The ground-based global navigation satellite system (GNSS) and the satellite-based interferometric synthetic aperture radar (InSAR) are efficient techniques for high-precision and high-resolution deformation monitoring (Cigna et al., 2021).

GNSS observations, acquired using both permanent and/or non-permanent stations (NPS), are characterized by high-precision and 3D information; however, the measurements are generally restricted to a few points due to the cost of sensors, data processing, installation and maintenance for the continuous stations, or are time-consuming in case of multitemporal repetition of the surveys on NPS (Yuwono and Prasetyo, 2018; Cenni et al., 2021). InSAR information provides high-precision and quasi-continuous data with resolution from medium to high, on the basis of the acquisition mode and the sensor used. The technique allows cost-effective monitoring of the Earth's surface (including structures/infrastructures) taking advantage of freely available open data (in particular, using Sentinel-1 imagery). On the other hand, the information is restricted to the line of sight (LOS) of the satellite (Motagh et al., 2007; Cigna et al., 2021; Wang et al., 2023; Karami et al., 2023). Even if descending and ascending orbits can be combined to extract east-west and up-down displacements, this procedure leads to a reduction in the density of the ground measurement points; for this reason, when the resolution of the points is a crucial issue, it is preferable to use descending and ascending orbits separately (Chen et al., 2021; Alonso-Díaz et al., 2024; Xiao et al., 2024). In terms of accuracy, similar values can be obtained using the two techniques. Uncertainties on the order of a few millimeters per year and about 1 cm per year are typical of continuous GNSS data and repeated GNSS measurements at NPS, respectively (Motagh et al., 2007; Fiaschi et al., 2018; Hu et al., 2018; Manunta et al., 2019; Chen et al., 2021; Cigna et al., 2021; Cigna and Tapete, 2021; Beattie et al., 2024; Yeh et al., 2025; Zhu et al., 2025). In most cases, the integration of the two techniques allow to mitigate their respective limitations (Casu et al., 2006; Qiu et al., 2023; Ellis et al., 2025). Many researchers have integrated GNSS data with InSAR velocities to study different phenomena. Among others, glacier monitoring in Iceland (Magnússon et al., 2011); correction of atmospheric errors using GPS meteorological data in SAR interferometry (Cheng et al., 2012); monitoring large deformations in coal mining of Daliu Tower in China (Chen et al., 2015); estimation of displacements of the Claudian Aqueduct in Rome, Italy (Tapete et al., 2015); evaluation of landslide movements in the Columbia River Gorge, US (Hu et al., 2018); analysis of vertical land deformations in northern Italy (Farolfi et al., 2019); studying land motion of Dubrovnik in Croatia (Grgić et al., 2020); detection of surface rupture generated by the 30 October 2016 earthquake in central Italy (Wilkinson et al., 2017); monitoring of deformations of the Corinth canal in Greece (Yaragunda and Oikonomou, 2024).

The level of agreement between InSAR and GNSS velocities can be improved by calibrating the satellite-based data using ground-based information. This approach was applied in different applications, including monitoring deformations of structures/infrastructures (Roque et al., 2021; Fabris and Floris, 2025) and land subsidence (Fabris et al., 2022; Ng et al., 2023; Deng and Zumberge, 2025).

Studying the reliability of these data is crucial, since the availability of satellite-based and ground-based sensors that acquire continuous data together with the near-real-time automatic processing is expected to increase in the next years; in this context, the calibration, validation and estimation of uncertainties of open datasets used by many researchers to study different phenomena pose a real challenge to obtain reliable data. An example is given by the European Ground Motion Service (European Environment Agency, 2025) of the Copernicus program and the Veneto Region (Italy) InSAR databases (Veneto Region, 2020).

For all these reasons, repeated GNSS measurements at 46 NPS together with observations from 3 Continuous GNSS (CGNSS) stations and InSAR velocities from EGMS and Veneto Region datasets were analyzed in this study to: i) evaluate the performance/quality of open interferometric data using ground-truth GNSS information; ii) monitor the land subsidence in the Po river delta (PRD, northern Italy, Figure 1) in the period 2018–2022.

The EGMS dataset used in this work was validated in 37 areas distributed throughout Europe comparing the data with site-specific information. The validation sites included landslides, mining and post-mining, groundwater over exploitation, active volcanic environments, and urban areas (Sala Calero et al., 2024). A comparison was made in PRD with the Veneto region InSAR dataset which provided a relative velocity difference for the identified active deformation areas of approximately 40%; these discrepancies were attributed to the regional dataset due to the smaller size of the processed area and the processing strategy focusing on local phenomena (Sala Calero et al., 2023; Sala Calero et al., 2024). However, since an *in situ* validation of the EGMS applied to land subsidence in a large delta environment is not available, a further comparison between the InSAR datasets with ground-based dense GNSS measurements in the PRD allows a complete validation of the interferometric data.

In detail, the aim of this work is to evaluate the level of agreement between ground-based and satellite-based data by calibrating the interferometric information using the GNSS velocities, and validating the obtained values with independent measurements; after calibration and validation, the GNSS and InSAR data were integrated to develop an effective monitoring system of the land subsidence in the PRD. GNSS information, used as ground truth, were obtained from the 49 points of the

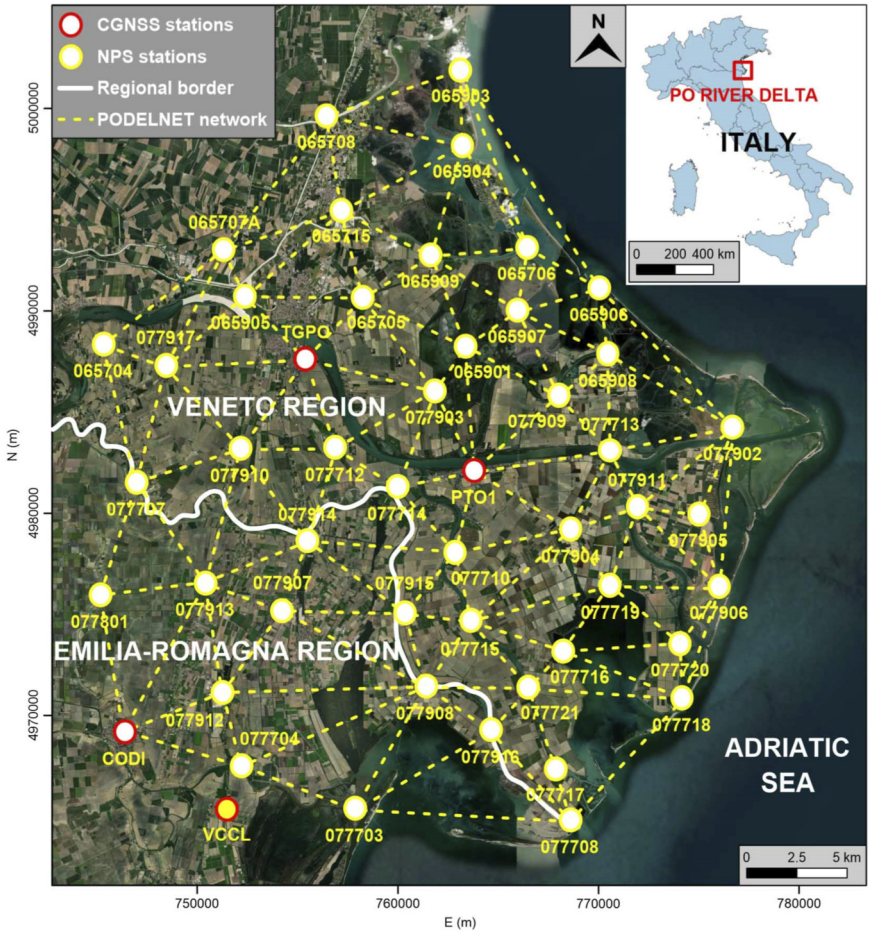

FIGURE 1
Location of the study area in northern Italy representing the continuous GNSS (CGNSS) and non-permanent site (NPS) stations, the connection between the points (generating the Po delta network–PODELNET), and the Veneto–Emilia Romagna regional border.

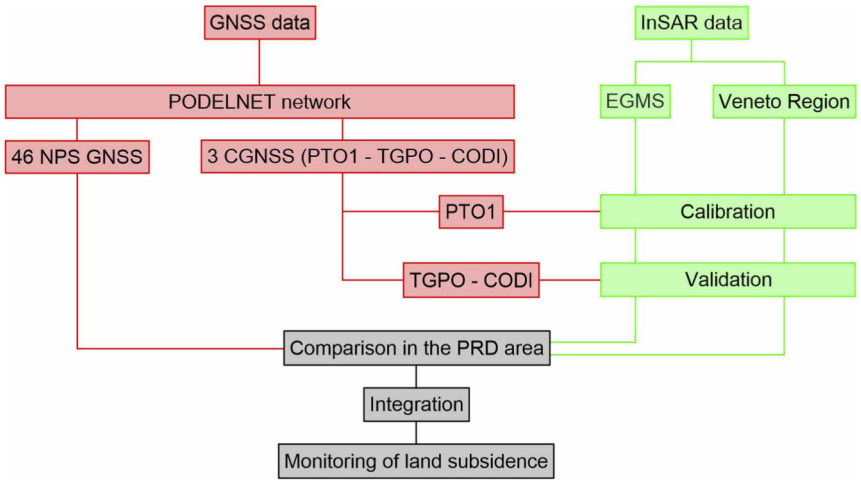

FIGURE 2
The flowchart used in this work for the calibration, validation, and integration of GNSS and InSAR velocities. Red represents the GNSS data, green highlights InSAR data and grey emphasize the comparison and integration of information.

TABLE 1 Main characteristics of the InSAR data from the EGMS and Veneto Region services used in this work.

Dataset	Orbit	Track	Scene	Period
EGMS	Ascending	44	265–266-267	13.06.2018–12.07.2022
	Ascending	117	264–265-266	12.06.2018–15.07.2022
	Descending	95	806–807-808	11.06.2018–14.07.2022
Veneto region	Ascending	117	Regional area	02.01.2019–15.07.2022
	Descending	95	Regional area	01.01.2019–14.07.2022

Po delta network (PODELNET), a network measured for the first time in 2016 and with surveys repeated each 2 years. The acquired observations were processed calculating the multitemporal coordinates of the 46 NPS points and the CGNSS stations of Porto Tolle (PTO1), Taglio di Po (TGPO), and Codigoro (CODI). The InSAR data from the EGMS and Veneto Region databases were then calibrated using the PTO1 continuous station, located in the center of the study area. Subsequently, the velocities before and after calibration were compared first with the TGPO and CODI CGNSS data, and secondarily with the 46 NPS GNSS information to provide a sensitivity test; therefore, the order of agreement between GNSS and InSAR velocities was estimated. Finally, the calibrated interferometric data were incorporated into the deformation monitoring system for measuring land subsidence in PRD (Figure 2).

This paper is organized as follows. Section 2 describes the study area, the acquisition and processing of GNSS data, the InSAR datasets, and the procedures adopted for calibration and validation. Section 3 provides the results obtained, and Section 4 discusses them, focusing on the comparison between the GNSS and InSAR velocities to estimate the level of agreement finalized to obtain reliable data, and to extract an efficient monitoring system of land subsidence. Finally, Section 5 summarizes the work and presents some conclusions.

2 Materials and methods

2.1 The study area and land subsidence

GNSS and InSAR data used in this study are related to the PRD area, located in northern Italy. It is a complex ecosystem where the Po, the longest Italian river, flows into the Adriatic Sea (Figure 1). The delta covers an area of about 400 km^2 and is a result of natural sedimentary processes and human activities (Carlo, 1998). A large portion is formed by reclaimed territories with shallow water bodies (Simeoni and Corbau, 2009).

The land subsidence in this area is a consequence of natural and anthropogenic factors. The natural contribution was derived from both the highly compressible Holocene deposits that cover the shallowest 30–40 m of the sedimentary sequence (Teatini et al., 2011) and tectonic deformations (Carminati et al., 2003; Picotti and Pazzaglia, 2008); the velocities linked to these effects, evaluated on the basis of geometric leveling and Global Positioning System (GPS) measurements (1950–2005 period) and InSAR data (1992–2005 period), are on the order of 2–4 mm/year (Carminati and Martinelli, 2002; Carminati et al., 2003; Teatini et al., 2011). The anthropogenic contribution was correlated with the extensive exploitation of non-confined, semi-confined, and confined acquifers (Martinelli et al., 2014); in the middle of the last century the velocities reached values from tens to hundreds of mm/year (Fabris, 2021). Studies of Teatini et al. (2011), Caputo et al. (1970), Caputo (1971), Simeoni and Corbau (2009), Corbau et al. (2019) using leveling measurements estimated land subsidence velocities of up to 300 mm/year in the period 1950–1957. The high rates of deformation led the Italian Government to suspend the extensive exploitation of the multi-aquifers system that started after the Second World War for industrial and agricultural uses together with the methane–water withdrawals from onshore and offshore reservoirs. The consequence was a progressive benefit of vertical settlement rates up to 30 mm/year in the period 1962–1974 (Caputo et al., 1970; Bondesan and Simeoni, 1983). Subsequently, land subsidence rates have continued to decline and, at present, the maximum values toward the sea are on the order of 10 mm/year (Fiaschi et al., 2018; Corbau et al., 2019; Fabris et al., 2022). During the last century, land subsidence largely modified the morphology of the PRD: currently, most of the area lies below the mean sea level with a very low sediment supply due to the artificial embankments built to prevent flooding and to increase the hydraulic safety of this fragile ecosystem (Correggiari et al., 2005).

2.2 GNSS observations and processing procedures

The GNSS observations derived from the multitemporal survey of the PODELNET network are made up of the 3 CGNSS stations of PTO1, TGPO, and CODI integrated with 46 NPS homogeneously distributed in the PRD, both in urbanized and rural areas (Figure 1). The network was developed and measured for the first time in 2016; the surveys were repeated every 2 years, requiring about 2 weeks each time, and the observations analyzed in this work were acquired in June/July 2016, 2018, 2020 and 2022. Due to the decommissioning of the CODI station in 2021, located at the network border, the Codigoro CGNSS station was replaced with the continuous VCCL station (Vaccolino) in the last measurement in 2022 (Figure 1). In each survey, the acquisitions were carried out adopting fixed settings: the same 130 baselines, with the same sampling rates of 15 s, minimum time stationing for each baseline of 3 h, and instruments (when possible) were used to reduce as much as possible the impact of the parameter settings on the estimation of the coordinates of the 46 NPS. While at the beginning GPS receivers were mostly used for data acquisition (two GPS Leica System 1200 and two GPS Leica System 500), over time new GNSS receivers were adopted (two GNSS Leica Viva–GS14 and CS15 – two GNSS Leica Viva–GS16 and CS20 – and a GNSS Topcon HiPer HR), collecting observations from GPS, GLONASS, GALILEO and BEIDOU constellations. In this way, the network was modified over time, from 'mostly GPS' to 'mostly GNSS'. In the processing of the baselines, all the available

FIGURE 3
Procedure for the comparison between the continuous/NPS GNSS and InSAR velocities in PRD. InSAR points enclosed in circles centered on the CGNSS station (placed in urbanized areas), with radii of 50 m, 100 m, 150 m and 200 m were selected **(a)**. In the case of NPS GNSS points, most of the time located in vegetated areas, the radius of the circle was fixed to the highest value of 200 m **(b)**. For each group of points, enclosed in the different circles, the LOS velocities were averaged and compared with the respective GNSS values.

TABLE 2 **Vertical velocities (VV) of the permanent stations calculated using the GNSS observations acquired during the PODELNET campaigns of 2016, 2018, 2020 and 2022. The values obtained in the period 2018–2022 were in agreement with those related to the global period 2016–2022.** *Velocities restricted to 2020.

Code	VV (2016–2022) (mm/year)	VV (2018–2022) (mm/year)
CODI*	−2.8 ± 1.8	−3.0 ± 1.7
PTO1	−5.3 ± 2.1	−5.2 ± 1.9
TGPO	−5.8 ± 1.8	−6.0 ± 2.0

constellations were selected obtaining, consequently, GPS and GNSS baselines.

The processing of the PODELNET network started from the coordinates of the 3 CGNSS stations. These values were obtained in a first phase, when the observations of the 3 continuous stations, acquired during the PODELNET measurements, were processed using the Bernese software together with the data of the Italian GNSS network. The latter is a network composed of about 600 permanent stations located in the Italian and surroundings areas. In this way, the positions of the 3 CGNSS stations were calculated in the ETRF2014 realization of the ITRF2014 reference frame: with this procedure, the horizontal Eurasian plate motion was removed (Altamimi et al., 2016). In a second phase, the GPS and GNSS baselines related to the minimum distance between the points of the PODELNET network were calculated for each survey using Leica Infinity software (yellow dashed lines in Figure 1). Subsequently, the network was adjusted and georeferenced using the 130 generated baselines that correspond to the sides of the triangles in Figure 1 and the coordinates of the three continuous stations previously calculated for each measurement. Finally, from the calculated coordinates of each point, both continuous and NPS, the velocities were extracted by means of the linear interpolation of the multitemporal data in the analyzed period.

2.3 InSAR datasets

In this work InSAR velocities obtained from the EGMS of the Copernicus program and the Veneto Region database were used. The two services provide open data referred to the LOS velocities extracted from Advanced-DInSAR processing (i.e., PS-InSAR, persistent scatterer InSAR, Ferretti et al., 2001, and SqueeSAR, Ferretti et al., 2011) of the interferometric images acquired by Sentinel-1.

The products provided by the EGMS were subdivided into: (i) Basic; (ii) Calibrated; (iii) Ortho (Crosetto et al., 2021). In this analysis, the Calibrated data were used; they were composed of points obtained from the processing of interferometric images acquired with the Sentinel-1 satellite. Compared to the Basic product, the Calibrated data were referenced using a model based on the European GNSS network. The points, measured along the LOS, were supplied with different attributes, including quality indexes, estimated mean velocity in the analyzed period, and time series of displacements. The spatial data covered the European Community and estimates the surface deformation rates with precision at the millimiter-level (Crosetto et al., 2025).

The Veneto Region Sentinel-1 PS (Permanent Scatterers) were made up of interferometric points obtained from the processing of Sentinel-1 images using the SqueeSAR technique. The available data provided the annual mean velocities of the PS and the displacement time series. The spatial data covered the Veneto Region, located in the northeast of Italy, and the service was mainly dedicated to civil protection issues.

Table 1 reports the details of the available InSAR data. Note that the Veneto Region InSAR datasets (January 2019 – July 2022 period) do not perfectly overlap with EGMS (June 2018 – July 2022) and GNSS information: the GNSS velocities were calculated by interpolating the positioning obtained from June/July 2018 to June/July 2022. This lack of temporal homogeneity between the datasets could make the direct comparison weaker. However, because land subsidence in this area was associated with the consolidation of late Holocene sediments, the linear trend of the deformation could be accepted (Teatini et al., 2011).

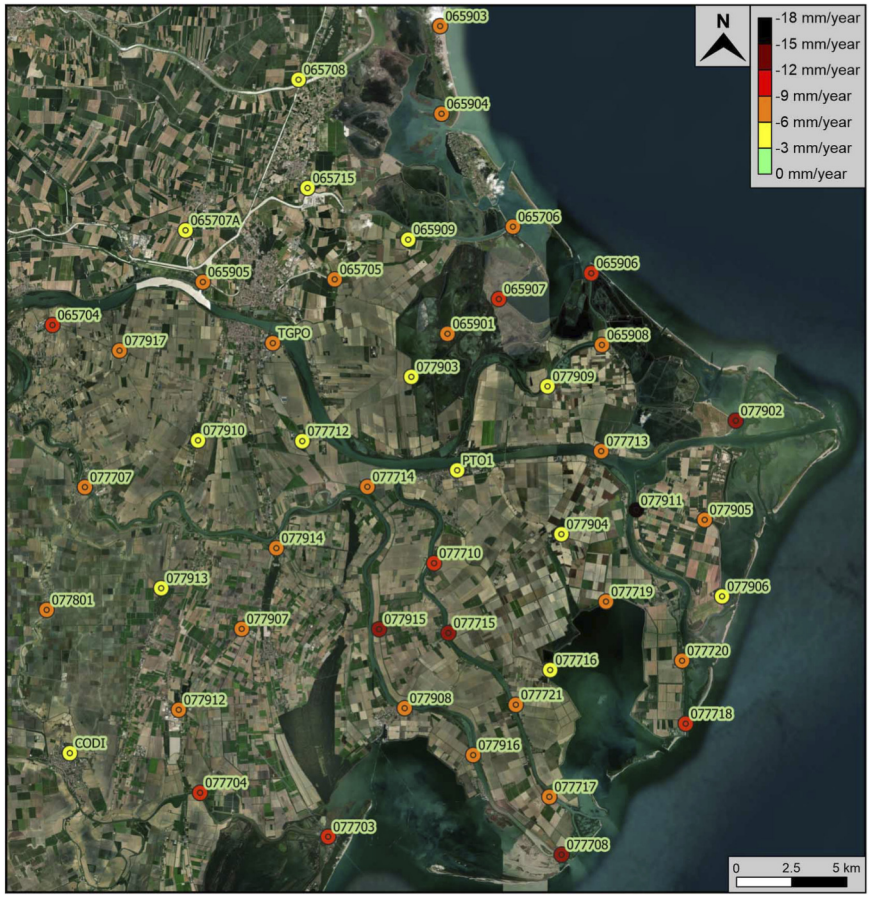

FIGURE 4
Vertical velocities of the CGNSS and NPS stations of the PODELNET network obtained by interpolating the elevations calculated from the surveys carried out in 2018, 2020 and 2022.

2.4 Calibration and validation of the InSAR data

EGMS and Veneto Region InSAR velocities were compared with GNSS data to calibrate and validate interferometric products in the PRD area; in this procedure, ground-based CGNSS measurements were considered more reliable (Cigna et al., 2021).

Many researchers studied and compared the results obtained from the two techniques to estimate the level of agreement. Root mean square error (RMSE) and/or standard deviation of differences lower than 1 cm can be achieved. Ng et al. (2023) integrated Sentinel-1 information with continuous GNSS velocities to evaluate land subsidence in Sydney. The authors compared the velocities obtaining a mean value of the differences lower than 1 mm/year and RMS of the order of 1 mm/year, but with some values greater than 2 mm/year. Huang et al. (2024) investigated the structural safety assessment of high buildings located in the Guangzhou–Foshan metropolitan area. They compared the velocities obtained from 45 InSAR points with the deformation velocity of the GUAN continuous GNSS station. The results provided an overall RMSE of 1.50 mm/year. The same value was suggested by Fiaschi et al. (2018) analysing Sentinel-1 InSAR imagery and CGNSS data from 2014 to 2017 in the Po river delta area (Italy). Consequently, the 1.5 mm/year value is adopted in this work to represent the reference uncertainty threshold in the evaluation of the agreement between the InSAR and GNSS velocities.

The calibration involved the continuous station PTO1 as a reference, because it was located in the center of the study area, where the EGMS and Veneto Region datasets were available (Figure 1). At this point, if a difference greater than the threshold value of 1.50 mm/year (absolute value) was found between the velocities of the InSAR points and the CGNSS value, the satellite-based data were calibrated. In this way, the PS velocities were aligned with the velocity of the PTO1 CGNSS station. In detail, comparisons were made by selecting the interferometric points enclosed in circles centered on the CGNSS station and with different radius, up to 200 m (Figure 3a). The mean value of their velocities was compared and then calibrated with the PTO1 GNSS velocity projected along the LOS of the satellite. The different radii were selected to evaluate the variability of the InSAR velocities for PSs closed to the CGNSS station (up to 50 m) compared to the mean rates of the interferometric points up to 100 m, 150 m, and 200 m from the PTO1 station. In this way, the comparison with the GNSS velocity projected along the LOS provided a more robust statistical value and an estimation of the variability of the velocities based on the spatial distribution of PSs.

TABLE 3 Comparison between the mean velocities of the EGMS PS points located up to 200 m from the permanent stations and the vertical velocities of the PTO1, TGPO, and CODI CGNSS stations projected along the LOS of the satellites; for each analyzed track, different locations of the PS points from the CGNSS station was considered: i) the closest point; ii) the mean value of the two closest points; iii) the mean value of the three closest points; iv) the mean value of the points located up to 50 m from the CGNSS station; v) the mean value of the points located up to 100 m from the CGNSS station; vi) the mean value of the points located up to 150 m from the CGNSS station; vii) the mean value of the points located up to 200 m from the CGNSS station.

CGNSS station	Distance from the station (m)	Track 44			Track 117			Track 95		
		N. Of PS	PS vel. (mm/year)	CGNSS vel. (mm/year)	N. Of PS	PS vel. (mm/year)	CGNSS vel. (mm/year)	N. Of PS	PS vel. (mm/year)	CGNSS vel. (mm/year)
PTO1	-	1	−4.5	−4.3 ± 0.4	1	−4.5	−3.9 ± 0.4	1	−3.3	−3.9 ± 0.4
	-	2	−4.2 ± 0.4		2	−4.8 ± 0.5		2	−3.1 ± 0.3	
	-	3	−4.3 ± 0.3		3	−4.3 ± 0.4		3	−3.2 ± 0.2	
	50	26	−4.2 ± 0.4		51	−4.5 ± 0.5		46	−3.5 ± 0.6	
	100	142	−4.4 ± 0.6		223	−4.5 ± 0.5		188	−3.4 ± 0.6	
	150	322	−4.4 ± 0.6		460	−4.6 ± 0.6		376	−3.4 ± 0.7	
	200	531	−4.4 ± 0.4		753	−4.6 ± 0.6		544	−3.4 ± 0.7	
TGPO	-	1	−3.7	−4.9 ± 0.6	1	−5.2	−4.5 ± 0.6	1	−2.7	−4.5 ± 0.6
	-	2	−3.6 ± 0.1		2	−4.8 ± 0.4		2	−3.0 ± 0.4	
	-	3	−3.7 ± 0.1		3	−4.8 ± 0.5		3	−2.8 ± 0.6	
	50	30	−4.0 ± 1.1		51	−5.0 ± 0.6		28	−3.9 ± 0.7	
	100	113	−4.2 ± 0.9		169	−5.1 ± 0.6		135	−3.9 ± 0.7	
	150	208	−4.1 ± 1.0		309	−5.1 ± 0.6		235	−4.0 ± 0.7	
	200	286	−4.1 ± 0.9		431	−5.1 ± 0.7		338	−3.9 ± 0.7	
CODI	-	-	-	−2.6 ± 0.5	1	−3.6	−2.4 ± 0.5	1	−2.4	−2.4 ± 0.5
	-	-	-		2	−4.2 ± 0.7		2	−2.9 ± 0.7	
	-	-	-		3	−4.7 ± 1.1		3	−2.8 ± 0.6	
	50	-	-		46	−3.8 ± 0.9		37	−2.6 ± 0.7	
	100	-	-		142	−3.8 ± 0.8		103	−2.5 ± 0.6	
	150	-	-		283	−3.9 ± 0.7		230	−2.6 ± 0.8	
	200	-	-		465	−4.0 ± 0.8		365	−2.7 ± 0.8	

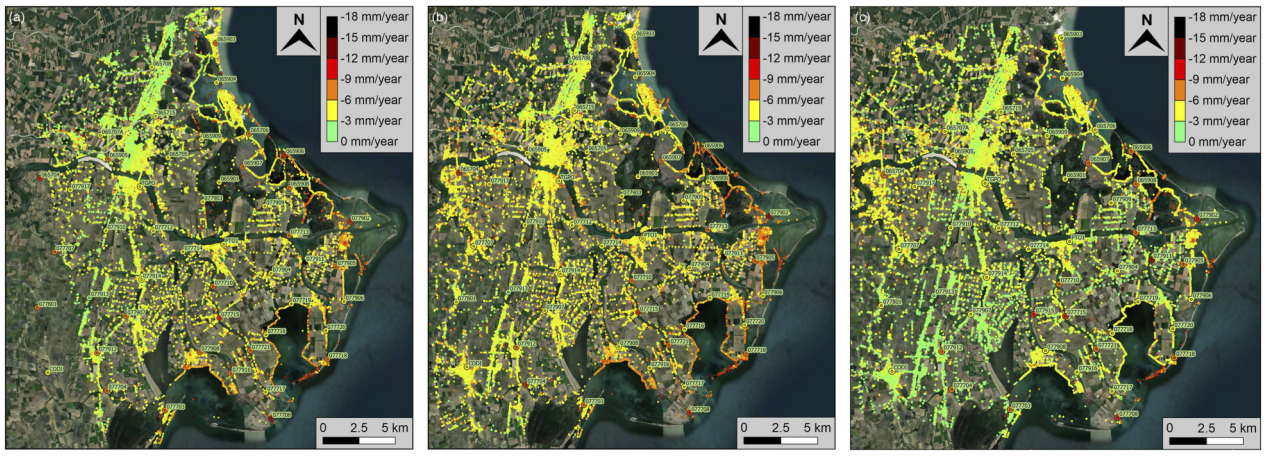

FIGURE 5
Kinematic pattern of LOS velocities in the PRD area integrating GNSS and EGMS InSAR data: **(a)** ascending track 44; **(b)** ascending track 117; **(c)** descending track 95.

TABLE 4 Differences in velocities between the vertical values of the PTO1, TGPO and CODI CGNSS stations projected along the LOS and the mean values of PSs with a maximum distance of 200 m from the permanent stations for the ascending tracks 44, 117, and the descending track 95 (EGMS dataset). The values obtained after calibration using the PTO1 reference station were also reported. BC: before calibration; AC: after calibration.

CGNSS station	Differences between velocities (CGNSS–InSAR) on LOS (mm/year)					
	Track 44		Track 117		Track 95	
	BC	AC	BC	AC	BC	AC
PTO1	0.1	0	0.7	0	−0.5	0
TGPO	−0.8	−0.9	0.6	−0.1	−0.6	−0.1
CODI	-	-	1.6	0.9	0.3	0.8

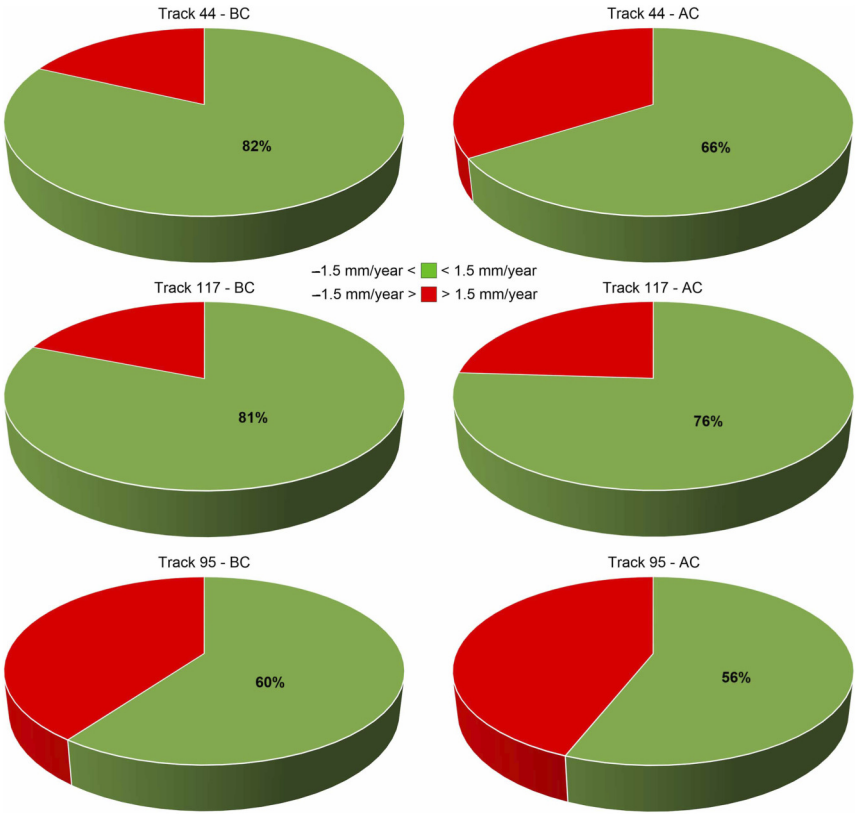

FIGURE 6
Classification of differences between velocities (PODELNET GNSS–InSAR) in percentages based on the threshold values of ±1.5 mm/year: for each track (ascending 44, 117, and descending 95 of the EGMS dataset), the values in the range ±1.5 mm/year were represented in green. BC: before calibration; AC: after calibration.

The projection along the LOS of the satellite was performed using the following equation:

$$V_{LOS} = V_V * \cos\theta \quad (1)$$

Where V_{LOS} indicate the projected GNSS velocity along the satellite LOS, V_V represents the vertical GNSS velocity and θ the incident angle, since the horizontal components of the velocities were negligible in the PRD area (Cenni et al., 2021). Negative values indicate land subsidence, i.e., increasing distance in the subsequent revisiting of the satellite. The incident angle used for each of the GNSS points was obtained from the InSAR data, considering the closest PS.

The validation phase was performed considering the available continuous stations, which were not used in the calibration process (TGPO and CODI). Since the GNSS velocities of the CODI station were restricted to July 2020, the comparison with the PS points was consequently limited, ensuring the time overlap between the datasets. In the subsequent surveys, the CODI station was replaced with the VCCL station, treated as a separate station.

In a second time, a sensitivity test was performed using the velocities of the 46 NPS of the PODELNET network. In particular, the mean velocities of the calibrated InSAR points, enclosed in a buffer zone centered on the NPS GNSS stations and with a radius of 200 m, were calculated. In this phase, the radius of the

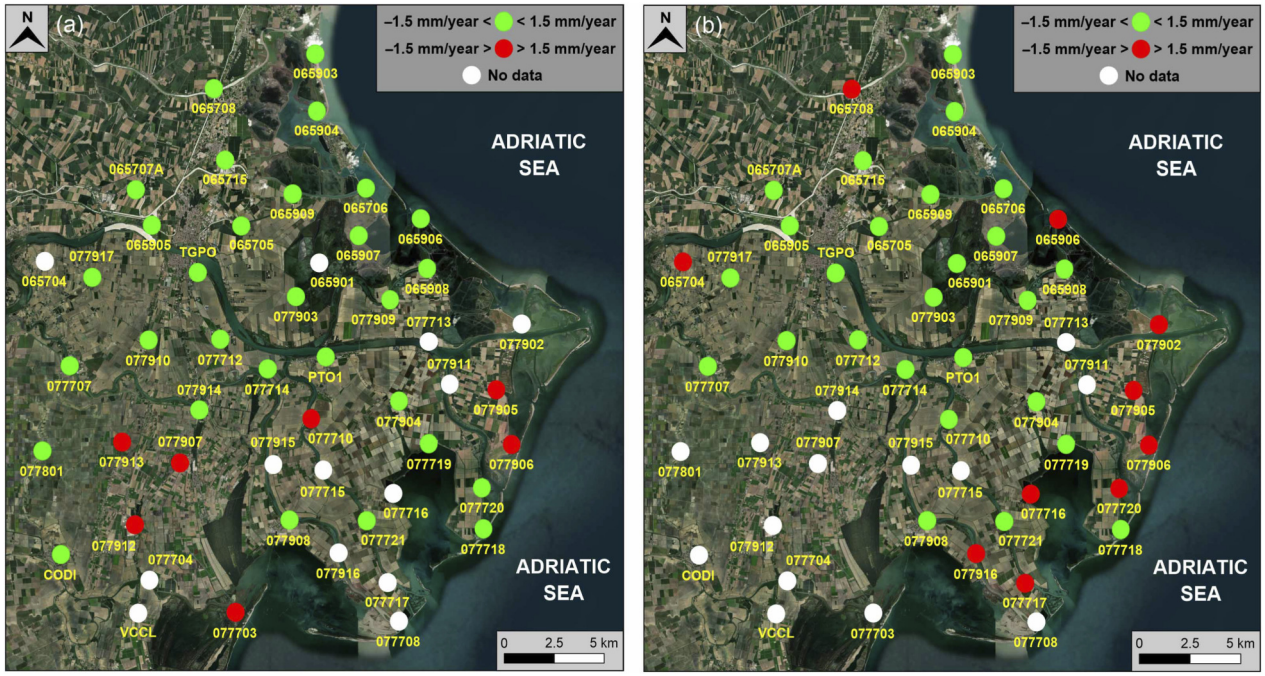

FIGURE 7
Spatial distribution of the differences between velocities: **(a)** GNSS–EGMS, ascending track 117; **(b)** GNSS–Veneto region, ascending track 117. The differences in the range ±1.5 mm/year are represented in green; the differences greater than the threshold values are highlighted in red; the GNSS points without PSs up to 200 m from the GNSS station are reported in white.

TABLE 5 **Comparison between the mean velocities of the Veneto Region PS points located up to 200 m from the permanent stations and the vertical velocities of the PTO1 and TGPO CGNSS stations projected along the LOS of the satellites. Note that the CODI station was located in the Emilia Romagna Region (Figure 1); for each analyzed track, different location of the PS points from the CGNSS station was considered: i) the closest point; ii) the mean value of the two closest points; iii) the mean value of the three closest points; iv) the mean value of the points located up to 50 m from the CGNSS station; v) the mean value of the points located up to 100 m from the CGNSS station; vi) the mean value of the points located up to 150 m from the CGNSS station; vii) the mean value of the points located up to 200 m from the CGNSS station.**

CGNSS station	Distance from the station (m)	Track 117			Track 95		
		N. Of PS	PS vel. (mm/year)	CGNSS vel. (mm/year)	N. Of PS	PS vel. (mm/year)	CGNSS vel. (mm/year)
PTO1	-	1	−0.8	−3.9 ± 0.4	1	−0.1	−3.9 ± 0.4
	-	2	−1.3 ± 0.4		2	−0.2 ± 0.1	
	-	3	−1.1 ± 0.3		3	−0.2 ± 0.1	
	50	4	−2.8 ± 3.1		6	−0.4 ± 0.4	
	100	21	−1.8 ± 1.5		21	−0.2 ± 0.5	
	150	43	−1.7 ± 1.2		39	−0.3 ± 0.6	
	200	76	−1.7 ± 1.4		56	−0.2 ± 0.6	
TGPO	-	1	−1.7	−4.5 ± 0.6	1	−1.0	−4.5 ± 0.6
	-	2	−1.1 ± 0.5		2	−1.2 ± 0.3	
	-	3	−1.5 ± 0.7		3	−0.8 ± 0.7	
	50	5	−2.5 ± 2.6		3	−0.8 ± 0.7	
	100	19	−1.6 ± 1.1		16	−0.6 ± 0.8	
	150	28	−1.6 ± 1.0		27	−0.6 ± 0.8	
	200	48	−1.6 ± 1.0		41	−0.5 ± 0.8	

TABLE 6 Differences in velocities between the vertical values of the PTO1 and TGPO CGNSS stations projected along the LOS and the mean values of PSs with a maximum distance of 200 m from the permanent stations for the ascending track 117 and the descending track 95 (Veneto Region dataset). The values obtained after calibration using the PTO1 reference station were also reported. BC: before calibration; AC: after calibration.

CGNSS station	Differences between velocities (CGNSS–InSAR) on LOS (mm/year)			
	Track 117		Track 95	
	BC	AC	BC	AC
PTO1	−2.2	0	−3.7	0
TGPO	−2.9	−0.7	−4.0	−0.3

buffer was set to the largest value because many of the NPS were located in vegetated areas, where interferometric points quickly lose coherence in the multi-temporal analysis, making InSAR points sparse (Figure 3b).

The differences were calculated before and after calibration to evaluate the performance of the corrected InSAR velocities. Finally, the GNSS LOS information, from both the continuous and NPS stations, were integrated with the calibrated interferometric data to generate maps of land subsidence in an integrated monitoring system of the deformation velocities in the PRD area.

3 Results

3.1 CGNSS and NPS velocities of the PODELNET network

CGNSS velocities were calculated using observations acquired in 2018, 2020, and 2022, during the surveys of the PODELNET network. The horizontal components of the deformation were very small; only the north-south provided values on the order of 1 mm/year, in agreement with a previous work (Cenni et al., 2021); this result, together with the limitations of the InSAR technique to detect the north-south component of the velocity (close to the flight direction of the satellite, as well known), allowed the analysis to be restricted only to the vertical velocities of the continuous stations. The results of the processing, reported in Table 2, showed similar values obtained analyzing all available observations and those acquired in the period 2018–2022, confirming the linearity of the land subsidence in this area (Teatini et al., 2011).

Subsequently, from the adjustment and georeferencing of the PODELNET network the velocities of the 46 NPS were obtained (Figure 4). While the uncertainties of the CGNSS velocities were in the order of 2 mm/year (Table 2), those related to the NPS rates were about double (3–5 mm/year).

NPS showed land subsidence in agreement with the values provided by the CGNSS stations in the central PRD area. The general trend of vertical deformations showed increasing values from the inland to the coast, with land subsidence rates up to −15/−18 mm/year. It should be noted that no points were obtained with velocities in the range of 0 ÷ −3 mm/year, confirming that land subsidence continues to affect the entire study area, without portions really stable.

3.2 Comparisons between the GNSS and InSAR velocities

3.2.1 EGMS InSAR velocities

The comparison between the vertical velocities of the PTO1, TGPO, and CODI CGNSS stations projected along the LOS of the satellites by using Equation 1 and the velocities of the EGMS PS points related to each analyzed track was performed considering the different locations of the interferometric points from the CGNSS stations: i) the closest point; ii) the mean value of the two closest points; iii) the mean value of the three closest points; iv) the mean value of the points located up to 50 m from the CGNSS station; v) the mean value of the points located up to 100 m from the CGNSS station; vi) the mean value of the points located up to 150 m from the CGNSS station; vii) the mean value of the points located up to 200 m from the CGNSS station (Table 3).

Table 3 showed a high level of stability of interferometric velocities using buffers centered on permanent stations and with radii from 50 m to 200 m. The comparison with the CGNSS LOS velocities demonstrated that calibration was not required for the EGMS data, since the differences for tracks 44 (Figure 5a), 117 (Figure 5b) and 95 (Figure 5c) were lower than the fixed threshold value of ±1.5 mm/year. In this way, the available EGMS information, together with the GNSS data, could be used to extract maps of land subsidence in an integrated monitoring system of the PRD area (Figure 5).

Nevertheless, since the CGNSS and InSAR velocities provided slightly different values in the PTO1 reference station, a further calibration could be applied. Taking into account buffers with radius of 200 m, which guaranteed the higher stability of the InSAR velocities, the calibration of the interferometric data allowed an improvement in agreement between velocities at the TGPO and CODI stations of validation, especially for the ascending track 117 (Table 4).

The 46 NPS GNSS stations of the PODELNET network were analyzed to provide a sensitivity test of the methodology. In Figure 6 the percentages of differences in the range ±1.5 mm/year are shown in green. A good level of agreement was obtained, since 82%, 81% and 60% of the differences between velocities for tracks 44, 117 and 95, respectively, were lower than the threshold value of ±1.5 mm/year. However, a recalibration using the PTO1 reference CGNSS station provided a decreased level of agreement between velocities with values of 76%, 66%, and 56%, respectively, for the three analyzed tracks, mainly due to the different accuracy of the NPS rates compared to the CGNSS velocities.

The spatial distribution of the differences between velocities is reported in Figure 7. In particular, Figure 7a provides the distribution of PODELNET points considering the differences between the vertical rates of the GNSS points projected along the LOS and the mean velocities of the ascending track 117 (EGMS data). Differences between velocities in the range ±1.5 mm/year are represented in green, while those greater than the threshold value are highlighted in red. Finally, in white are reported the PODELNET

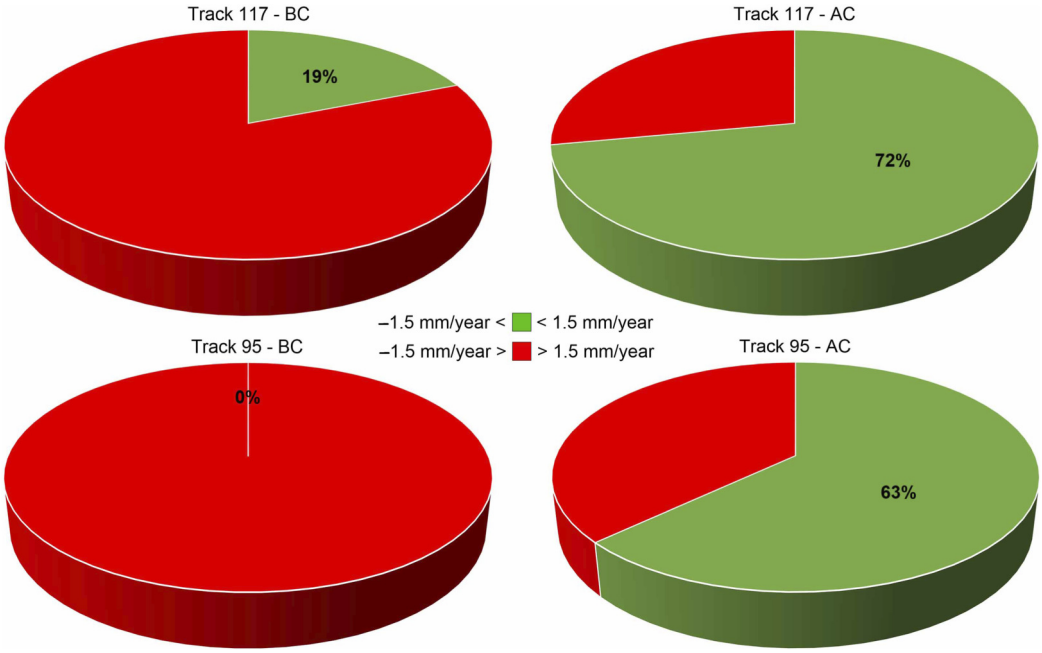

FIGURE 8
Classification of differences between velocities (PODELNET GNSS–InSAR) in percentages based on the threshold values of ±1.5 mm/year: for each track (ascending 117 and descending 95 of the Veneto Region dataset), values in the range ±1.5 mm/year were represented in green. BC: before calibration; AC: after calibration.

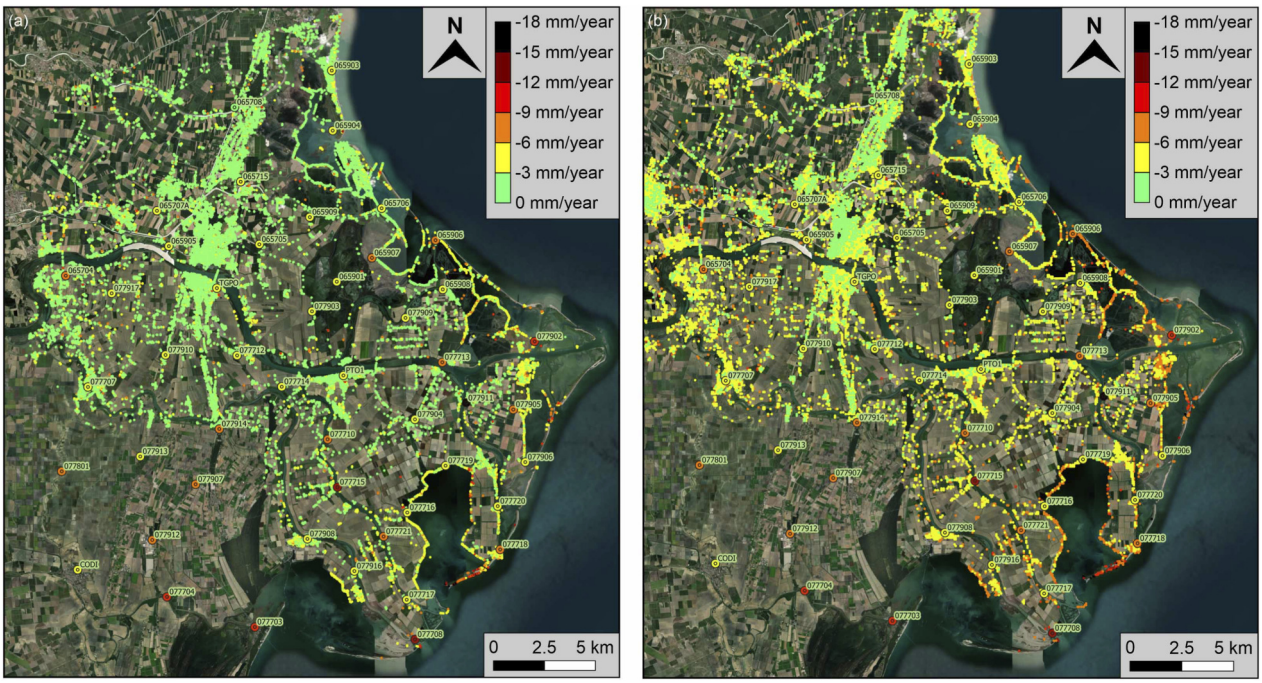

FIGURE 9
Kinematic pattern of LOS velocities in the PRD area integrating GNSS and Veneto Region InSAR data (ascending track 117): **(a)** Before Calibration; **(b)** After Calibration. Note that the ascending track 117 of the InSAR data was restricted to the Veneto Region (Figure 1).

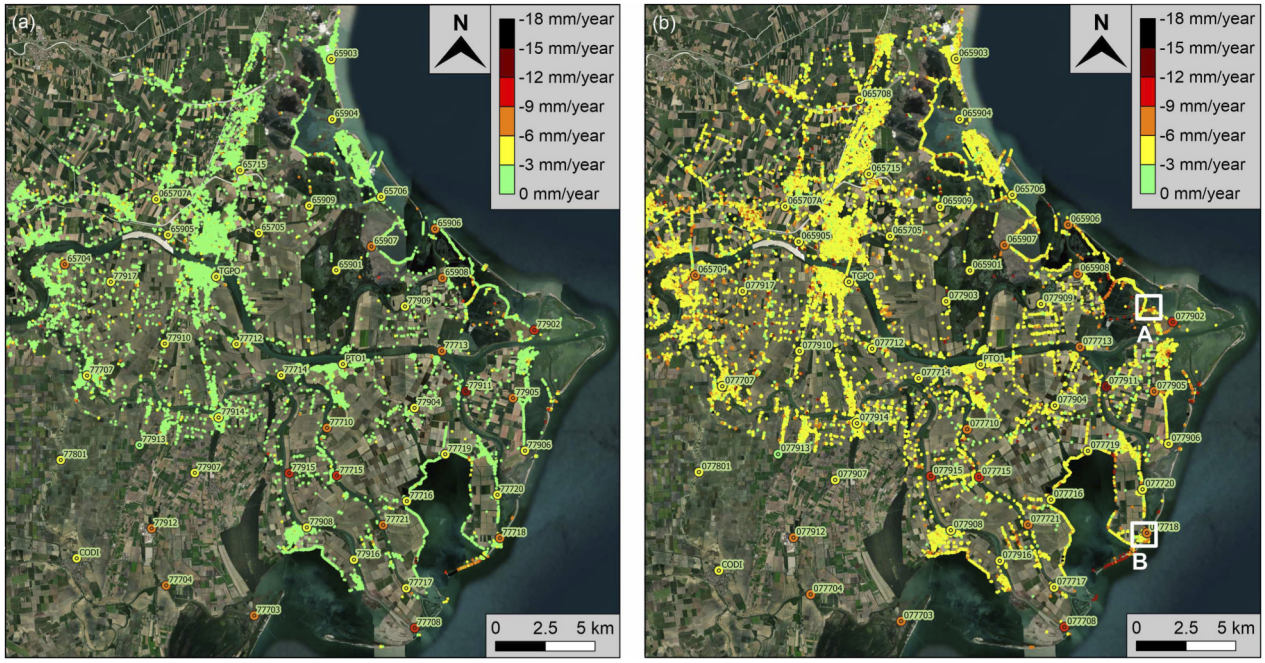

FIGURE 10
Kinematic pattern of LOS velocities in the PRD area integrating GNSS and Veneto Region InSAR data (descending track 95): **(a)** Before Calibration; **(b)** After Calibration. Note that the descending track 95 of the InSAR data was restricted to the Veneto Region (Figure 1).

points where the distance between the GNSS point and the PSs was greater than 200 m.

3.2.2 Veneto region InSAR velocities

The approach used for the EGMS data was applied for the Veneto Region InSAR information. The comparison between the vertical velocities of the PTO1 and TGPO CGNSS stations projected along the LOS of the satellites and the velocities of the Veneto region PS points related to tracks 117 and 95 was performed considering the different locations of the interferometric points from the CGNSS stations: i) the closest point; ii) the mean value of the two closest points; iii) the mean value of the three closest points; iv) the mean value of the points located up to 50 m from the CGNSS station; v) the mean value of the points located up to 100 m from the CGNSS station; vi) the mean value of the points located up to 150 m from the CGNSS station; vii) the mean value of the points located up to 200 m from the CGNSS station (Table 5).

Table 5 showed a high level of stability of interferometric velocities using buffers centered on permanent stations and with radii from 100 m to 200 m. The comparison with CGNSS LOS velocities demonstrated that calibration was necessary for Veneto Region data, as the differences for both tracks 117 and 95 exceeded the fixed threshold values of ±1.5 mm/year (Table 6).

In the sensitivity test the mean velocities of PSs with a maximum distance of 200 m from each of the 46 NPSs of the PODELNET network were compared with the vertical rates of the GNSS points projected along the LOS. The calculation was performed using the interferometric velocities available before and after calibration. In Figure 8 the percentages of differences in the range ±1.5 mm/year are shown in green. In this case, the level of agreement was very low, since only 19%, and 0% of the differences between velocities for tracks 117 and 95, respectively, were lower than the threshold value of ±1.5 mm/year. A recalibration using the PTO1 reference CGNSS station provided an increased level of agreement between velocities with values of 72% and 63%, respectively, for the two analyzed tracks.

Figure 7b provides the distribution of PODELNET points considering the differences between the vertical rates of the GNSS points projected along the LOS and the calibrated mean velocities of the ascending track 117 (Veneto region data). Differences between velocities in the range ±1.5 mm/year are represented in green, while those greater than the threshold values are highlighted in red. Finally, in white are reported the PODELNET points where the distance between the GNSS point and the PSs was greater than 200 m.

The calibration of the Veneto Region interferometric data significantly changed the deformation pattern of the study area, for both the ascending track 117 (Figure 9) and the descending track 95 (Figure 10). Figure 9a shows the distribution of velocities related to PS points, ascending track 117 (restricted to the Veneto region), together with the PODELNET GNSS rates projected along the LOS of the satellite. Figure 9b shows the same distribution, but with calibrated velocities applied to the interferometric PS points. Similarly, Figure 10a shows the distribution of velocities related to the PS points, descending track 95 (restricted to the Veneto region), together with the PODELNET GNSS rates projected along the LOS of the satellite. Figure 10b shows the same distribution, but with calibrated velocities applied to the interferometric PS points.

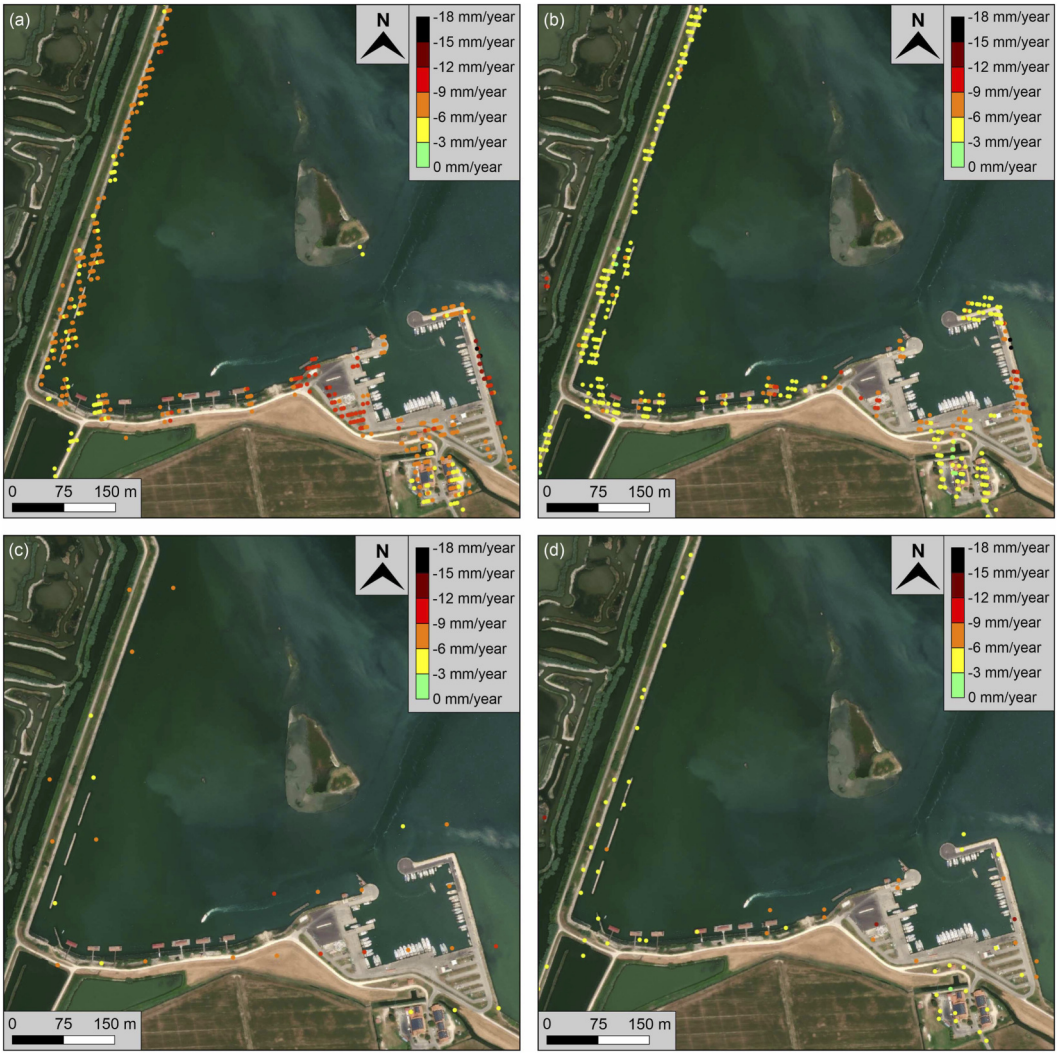

FIGURE 11
Detailed LOS velocities (both GNSS and InSAR) related to Pila port and the west portion of the sea embankment (area A of Figure 9b): **(a)** EGMS, track 117; **(b)** EGMS, track 95; **(c)** Veneto Region, track 117; **(d)** Veneto Region, track 95.

4 Discussion

4.1 Calibration and validation of InSAR data using ground-based GNSS information

The analysis of Table 5 highlights that, compared to the EGMS data (Table 3), using Veneto region dataset the number of detected PSs in each buffer was very different, justifying the stability of velocities obtained only using buffers with radius of at least 100 m.

Taking into account buffers with radius of 200 m, that guaranteed the higher stability of the Veneto region InSAR velocities, the calibration of the interferometric data performed in the PTO1 reference station provided a significant improvement in the agreement between velocities in the TGPO station of validation, since the differences fully fall within the threshold values (Table 6).

Figure 6, representing the percentages of the differences between velocities in the range ±1.5 mm/year in green (PODELNET GNSS–EGMS InSAR), provided changed values after calibration using the reference PTO1 CGNSS station. While calibration slightly improved the level of agreement between velocities at permanent stations (CGNSS LOS and interferometric velocities were very similar even without calibration, Table 4), this result was not confirmed at the NPS, where the percentages of differences in the range ±1.5 mm/year decreased in all tracks, especially for track 44. It should be noted that the velocities of CGNSS and NPS were characterized by different accuracies. Therefore, further calibration did not improve the velocities, confirming that an additional correction of the EGMS interferometric data was not necessary.

On the contrary, Figure 8, which represents the percentages of differences between velocities in the range ±1.5 mm/year in green (PODELNET GNSS–Veneto Region InSAR), provided an increasing percentage of points within the used range after calibration. In this case, the calibration not only improved the InSAR velocities in the validation TGPO station (Table 6), but allowed a significant improvement of the agreement between the velocities in the NPS, with final percentages comparable with those obtained using the

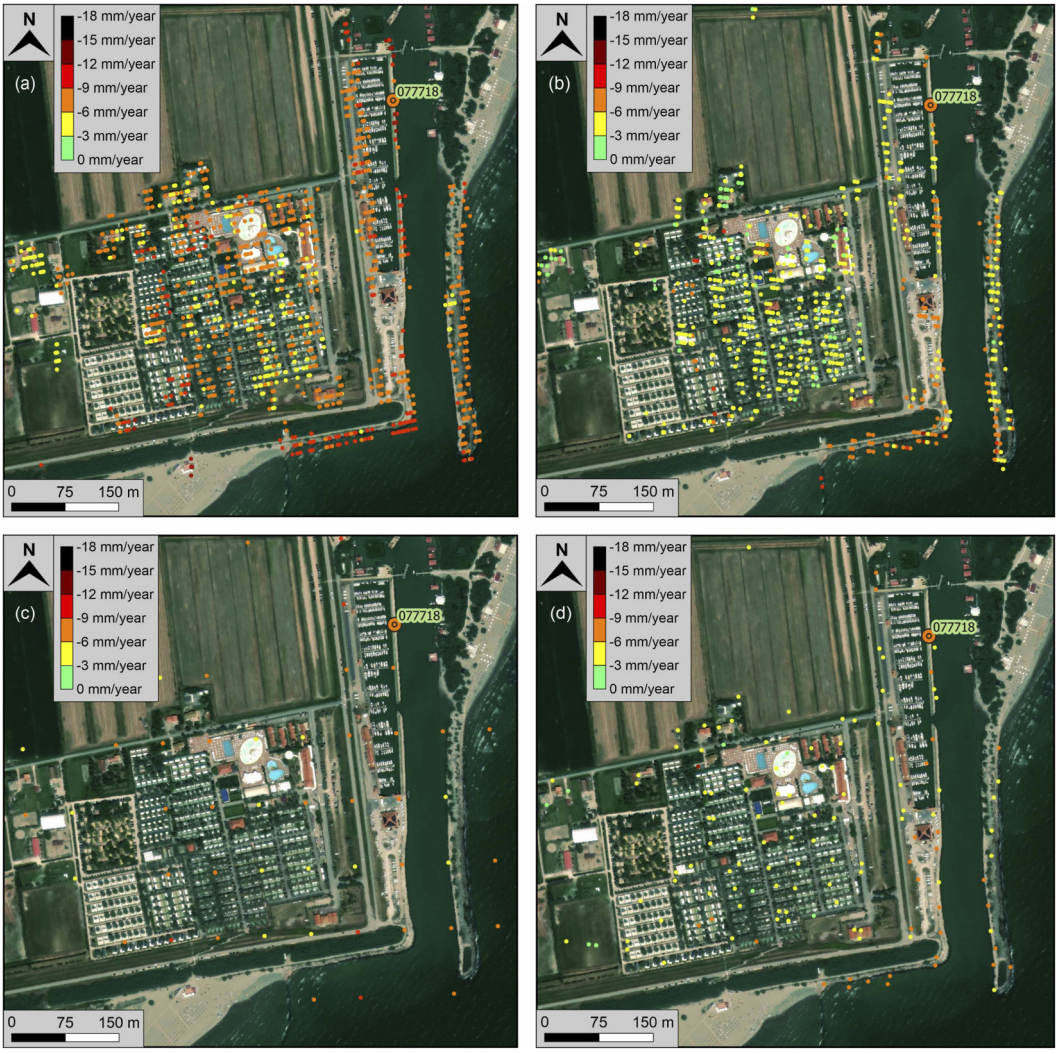

FIGURE 12
Detailed LOS velocities (both GNSS and InSAR) related to the village and port of Barricata and the defence sea embankments (area B of Figure 9b): **(a)** EGMS, track 117; **(b)** EGMS, track 95; **(c)** Veneto Region, track 117; **(d)** Veneto Region, track 95.

EGMS data (Figure 6). It should be noted that without calibration only 19% of the NPS provided differences between velocities in the range ±1.5 mm/year for track 117, and 0% for track 95. Based on these results, the calibration of the Veneto Region InSAR velocities using ground-based GNSS information is strongly recommended.

The PODELNET points outside the defined range of ±1.5 mm/year (red percentages in Figures 6, 8, red points in Figures 7a,b), representing points with significant differences between velocities (PODELNET GNSS–InSAR data), were due to: i) local deformations of the PODELNET points (e.g., for anthropic activities), because the GNSS data were related to specific points, while the InSAR measurements were based on the pixel size of the interferometric images; ii) noise or bias due to possible problems that occurred during the PODELNET measurements; iii) distances on the order of 200 m between the PODELNET points and the available PSs points, representing possible different deformations.

The spatial distribution of these points shows a different pattern considering EGMS data (Figure 7a) or Veneto region information (Figure 7b); while the differences between velocities that involved EGMS, track 117, were located in the southern part of the PRD, those related to the Veneto region, track 117, were mainly placed along the coast. 077,905 and 077,906 were in common, suggesting possible problems that occurred during the GNSS measurements. Additionally, four NPS points (065,708, 065,906, 077,710, and 077,720) modified the agreement/disagreement status using EGMS or Veneto region datasets.

4.2 Integrated monitoring system of land subsidence in PRD

Figure 5 represents land subsidence velocities obtained using tracks 44 (Figure 5a), 117 (Figure 5b) and 95 (Figure 5c) of the EGMS dataset integrated with the continuous and NPS GNSS points of the PODELNET network. The general trend

of movements showed increasing deformations from west to east, with LOS velocities ranging from 0/−3 mm/year to about −15 mm/year along the coastal area, in agreement with previous works (Fiaschi et al., 2018; Fabris et al., 2022) and the results obtained by Tosi et al. (2016), Deng and Zumberge (2025). However, the descending track 95 underestimates the velocities in the central-south and south-east portions of the PRD compared to the ascending tracks 44, 117, and the GNSS information. The calibrated velocities of the Veneto Region dataset, ascending track 117 (Figure 9b), provided a similar trend to the EGMS data, ascending track 117 (Figure 5b). On the other hand, the calibrated velocities of the descending track 95 (Figure 10b) were similar to those of the ascending track 117 (Figure 9b) in the area under investigation, with the exception of the coastal portion, where the trend was underestimated as in the descending track 95 of the EGMS data (Figure 5c).

A detailed analysis was performed in coastal areas A and B of Figure 10b, as an example. Area A describes the deformations of Pila port and the west portion of the sea embankment using tracks 117 and 95 of both EGMS and Veneto Region InSAR data (Figure 11).

Since the incident angle of the interferometric tracks analysed was very similar (differences lower than 1°), the LOS velocities were comparable. EGMS and calibrated Veneto Region InSAR data provided a similar deformation pattern using track 117 (Figures 11a,c) and track 95 (Figures 11b,d); the most significant difference was the number of PSs, which was very low in the regional dataset (see also Tables 3, 5). Once again, the information of track 95 underestimated the LOS velocities of land subsidence (Figure 11b). The deformations detected in this area were generally on the order of −6/−9 mm/year; however, in some structures of the Pila port, the movements were significant, with values up to −12/−15 mm/year.

Similar considerations can be extended for area B of Figure 10b, which describes the LOS deformations of the village and port of Barricata and the defence sea embankments (Figure 12).

LOS deformations detected in area B ranged, generally, from −3 mm/year to −9 mm/year. Higher values, up to −12/−15 mm/year, were identified along some portions of the coastline, probably caused by coastal erosion.

Figures 5, 9b, 10b provided LOS velocities of sea embankments along the PRD coastal area in the order of −6/−9/−12 mm/year: this result, accelerated by the rise in sea level due to climate changes (Antonioli et al., 2017; Rizzo et al., 2025), increases the risk of flooding in this area, largely below the mean sea level. For this reason, continuous monitoring of deformations together with the implementation of risk mitigation strategies are crucial activities for the protection and safeguard of the PRD.

5 Conclusion

In this work ground-based GNSS information from 3 continuous stations and 46 NPS of the PODELNET network were used to calibrate, validate, and integrate the InSAR data available from the EGMS of the Copernicus program and the Veneto Region databases for the monitoring of land subsidence in the PRD.

In a first phase, the PTO1 CGNSS station, located in the center of the PRD study area, was used to calibrate the interferometric velocities of the EGMS (ascending tracks 44 and 117, and descending track 95) and the Veneto Region (ascending track 117 and descending track 95) datasets. Based on the results reported by many authors, a threshold value of 1.5 mm/year in the differences between the velocities was used: in case of a difference greater than the threshold value, the calibration was applied, adjusting the interferometric velocities with the ground-based information; otherwise, the calibration was not applied. The TGPO and CODI CGNSS stations were used for validation. In this way, the Veneto Region InSAR data were calibrated.

In a second phase, the calibrated InSAR velocities of the EGMS and Veneto Region datasets were compared with the 46 NPS GNSS points of the PODELNET network to provide a sensitivity test of the applied methodology. The results highlighted that if a further calibration had been applied to the EGMS information, a decrease in the number of NPS with differences between velocities in the range ±1.5 mm/year would have been obtained (CGNSS and NPS velocities were characterized by different accuracies). On the contrary, the calibration applied to the Veneto Region InSAR data improved by about 60% the number of NPS with differences between velocities in the range ±1.5 mm/year.

Finally, based on the results obtained in this work, the EGMS InSAR data of the Copernicus program do not require further calibration in the PRD area. On the contrary, the Veneto Region InSAR velocities required calibration, both for the ascending track 117 and the descending track 95.

Calibrated and validated data were used to generate maps of land subsidence in an integrated monitoring system of the study area. Ground-based GNSS velocities and satellite-based interferometric information provided increasing land subsidence rates from west to east of the PRD; maximum LOS values, up to −15 mm/year, were obtained along the coastal area, where sea embankments that protect the inland largely below the mean sea level, are exposed to increasing risks of instability, accelerated by the sea level rise caused by the ongoing climate change.

Data availability statement

The original contributions presented in the study are included in the article/supplementary material, further inquiries can be directed to the corresponding author.

Author contributions

MF: Funding acquisition, Writing – review and editing, Project administration, Resources, Software, Formal Analysis, Writing – original draft, Conceptualization, Methodology, Validation, Data curation, Supervision, Visualization, Investigation. SN: Validation, Visualization, Writing – review and editing, Investigation, Methodology, Software, Formal Analysis.

Funding

The author(s) declared that financial support was not received for this work and/or its publication.

Acknowledgements

The authors would like to thank the "Laboratory of Geomatics and Surveying" staff at the University of Padova.

Conflict of interest

The author(s) declared that this work was conducted in the absence of any commercial or financial relationships that could be construed as a potential conflict of interest.

Generative AI statement

The author(s) declared that generative AI was not used in the creation of this manuscript.

Any alternative text (alt text) provided alongside figures in this article has been generated by Frontiers with the support of artificial intelligence and reasonable efforts have been made to ensure accuracy, including review by the authors wherever possible. If you identify any issues, please contact us.

Publisher's note

All claims expressed in this article are solely those of the authors and do not necessarily represent those of their affiliated organizations, or those of the publisher, the editors and the reviewers. Any product that may be evaluated in this article, or claim that may be made by its manufacturer, is not guaranteed or endorsed by the publisher.

References

Alonso-Díaz, A., Solla, M., Rodríguez, J. L., and Elseicy, A. (2024). Integrated approach to improve road infrastructure Resilience through complementary Non-Destructive Techniques, *Remote Sens. Spatial Inf. Sci.* 9–15. doi:10.5194/isprs-annals-X-4-W5-2024-9-2024

Altamimi, Z., Rebischung, P., Métivier, L., and Collilieux, X. (2016). ITRF2014: a new release of the International Terrestrial Reference Frame modeling nonlinear station motions. *J. Geophys. Res. Solid Earth* 121, 6109–6131. doi:10.1002/2016JB013098

Antonioli, F., Anzidei, M., Amorosi, A., Lo Presti, V., Mastronuzzi, G., Deiana, G., et al. (2017). Sea-level rise and potential drowning of the Italian coastal plains: flooding risk scenarios for 2100. *Quat. Sci. Rev.* 158, 29–43. doi:10.1016/j.quascirev.2016.12.021

Beattie, A., Ahmed, M., Chu, T., Gebremichael, E., Elshalkany, M., and Abdelrehim, R. (2024). Temporal gravimetry, campaign and permanent GNSS, and interferometric radar techniques: a comparative approach to quantifying land deformation rates in coastal Texas. *Sci. Total Environ.* 956, 177280. doi:10.1016/j.scitotenv.2024.177280

Bondesan, M., and Simeoni, V. (1983). Dinamica e analisi mortologica statistica dei litorali del delta del Po e alle foci dell'Adige e del Brenta. *Mem. Degli Ist. Geol. Mineral. Dell'Universita Padova* 36, 1–48.

Caputo, M. (1971). "Survey and geometric analysis of the phenomena of subsidence in the Region of Venice and its hinterland; Consiglio Nazionale delle ricerche," in *Laboratorio per lo Studio Della Dinamica Delle Grandi Masse: roma, Italy*.

Caputo, C., Pieri, M., and Unguendoli, R. (1970). "Geometric investigation of the subsidence in the Po Delta; Consiglio Nazionale delle ricerche," in *Laboratorio per lo Studio Della Dinamica Delle Grandi Masse: roma, Italy*.

Carlo, C. (1998). Physical processes and human activities in the evolution of the Po Delta, Italy. *J. Coast. Res.* 14, 775–793.

Carminati, E., and Martinelli, G. (2002). Subsidence rates in the Po Plain, northern Italy: the relative impact of natural and anthropogenic causation. *Eng. Geol.* 66, 241–255. doi:10.1016/s0013-7952(02)00031-5

Carminati, E., Martinelli, G., and Severi, P. (2003). Influence of glacial cycles and tectonics on natural subsidence in the Po Plain (Northern Italy): insights from 14C ages. *Geochem. Geophys. Geosystems* 4. doi:10.1029/2002gc000481

Casu, F., Manzo, M., and Lanari, R. (2006). A quantitative assessment of the SBAS algorithm performance for surface deformation retrieval from DInSAR data. *Remote Sens. Environ.* 102, 195–210. doi:10.1016/j.rse.2006.01.023

Cenni, N., Fiaschi, S., and Fabris, M. (2021). Monitoring of land subsidence in the Po River Delta (Northern Italy) using geodetic networks. *Remote Sens.* 13, 1488. doi:10.3390/rs13081488

Chen, B., Deng, K., Fan, H., and Yu, Y. (2015). Combining SAR interferometric phase and intensity information for monitoring of large gradient deformation in coal mining area. *Eur. J. Remote Sens.* 48, 701–717. doi:10.5721/EuJRS20154839

Chen, X., Achilli, V., Fabris, M., Menin, A., Monego, M., Tessari, G., et al. (2021). Combining Sentinel-1 interferometry and ground-based geomatics techniques for monitoring buildings affected by mass movements. *Remote Sens.* 13, 452. doi:10.3390/rs13030452

Cheng, S., Perissin, D., Lin, H., and Chen, F. (2012). Atmospheric delay analysis from GPS meteorology and InSAR APS. *J. Atmos. Sol.-Terr. Phys.* 86, 71–82. doi:10.1016/j.jastp.2012.06.005

Cigna, F., and Tapete, D. (2021). Present-day land subsidence rates, surface faulting hazard and risk in Mexico City with 2014–2020 Sentinel-1 IW InSAR. *Remote Sens. Environ.* 253, 1–19. doi:10.1016/j.rse.2020.112161

Cigna, F., Ramírez, R. E., and Tapete, D. (2021). Accuracy of Sentinel-1 PSI and SBAS InSAR displacement velocities against GNSS and geodetic leveling monitoring data. *Remote Sens.* 13, 4800. doi:10.3390/rs13234800

Corbau, C., Simeoni, U., Zoccarato, C., Mantovani, G., and Teatini, P. (2019). Coupling land use evolution and subsidence in the Po Delta, Italy: revising the past occurrence and prospecting the future management challenges. *Sci. Total Environ.* 654, 1196–1208. doi:10.1016/j.scitotenv.2018.11.104

Correggiari, A., Cattaneo, A., and Trincardi, F. (2005). The modern Po Delta system: Lobe switching and asymmetric prodelta growth. *Mar. Geol.* 222, 49–74. doi:10.1016/j.margeo.2005.06.039

Crosetto, M., Solari, L., Balasis-Levinsen, J., Bateson, L., Casagli, N., Frei, M., et al. (2021). Deformation monitoring at European scale: the copernicus ground motion service. *Int. Arch. Photogramm. Remote Sens. Spat. Inf. Sci.* 2021, 141–146. doi:10.5194/isprs-archives-XLIII-B3-2021-141-2021

Crosetto, M., Crippa, B., Mróz, M., Cuevas-González, M., and Shahbazi, S. (2025). Applications based on EGMS products: a review. *Remote Sens. Appl. Soc. Environ.* 37, 101452. doi:10.1016/j.rsase.2025.101452

Deng, F., and Zumberge, M. (2025). Seafloor motion from offshore man-made structures using satellite radar images—A case study in the Adriatic Sea. *Remote Sens. Environ.* 318, 114543. doi:10.1016/j.rse.2024.114543

Ellis, A. P., Johanson, I. A., and Poland, M. P. (2025). Deformation of Mauna Loa before, during, and after its 2022 eruption. *Bull. Volcanol.* 87, 8. doi:10.1007/s00445-024-01788-8

European Environment Agency (2025). *European ground motion service*. Available online at: https://egms.land.copernicus.eu/ (Accessed September 10, 2025).

Fabris, M. (2021). Monitoring the coastal changes of the Po River Delta (Northern Italy) since 1911 using archival cartography, MultiTemporal aerial photogrammetry and LiDAR data: implications for coastline changes in 2100 A.D. *Remote Sens.* 13, 529. doi:10.3390/rs13030529

Fabris, M., and Floris, M. (2025). Integrated GNSS and InSAR analysis for monitoring the shoulder structures of the MOSE System in Venice, Italy. *Remote Sens.* 17, 1059. doi:10.3390/rs17061059

Fabris, M., Battaglia, M., Chen, X., Menin, A., Monego, M., and Floris, M. (2022). An integrated InSAR and GNSS approach to monitor land subsidence in the Po River Delta (Italy). *Remote Sens.* 14, 5578. doi:10.3390/rs14215578

Farolfi, G., Bianchini, S., and Casagli, N. (2019). Integration of GNSS and satellite InSAR data: derivation of fine-scale vertical surface motion maps of Po Plain, Northern Apennines, and Southern Alps, Italy. *IEEE Trans. Geosci. Remote Sens.* 57, 319–328. doi:10.1109/TGRS.2018.2854371

Ferretti, A., Prati, C., and Rocca, F. (2001). Permanent scatterers in SAR interferometry. *IEEE Trans. Geosci. Remote Sens.* 39, 8–20. doi:10.1109/36.898661

Ferretti, A., Fumagalli, A., Novali, F., Prati, C., Rocca, F., and Rucci, A. (2011). A new Algorithm for processing interferometric Data-Stacks: SqueeSAR. *IEEE Trans. Geosci. Remote Sens.* 49, 3460–3470. doi:10.1109/TGRS.2011.2124465

Fiaschi, S., Fabris, M., Floris, M., and Achilli, V. (2018). Estimation of land subsidence in deltaic areas through differential SAR interferometry: the Po River Delta case study (Northeast Italy). *Int. J. Remote Sens.* 39, 8724–8745. doi:10.1080/01431161.2018.1490977

Grgić, M., Bender, J., and Bašić, T. (2020). Estimating vertical land motion from remote sensing and in-situ observations in the Dubrovnik area (Croatia): a multi-method case Study. *Remote Sens.* 12, 3543. doi:10.3390/rs12213543

Hu, X., Lu, Z., Pierson, T. C., Kramer, R., and George, D. L. (2018). Combining InSAR and GPS to determine transient movement and thickness of a seasonally active low-gradient translational landslide. *Geophys. Res. Lett.* 45, 1453–1462. doi:10.1002/2017GL076623

Huang, D., Qi, Z., Lin, S., Gu, Y., Song, W., and Lv, Q. (2024). Investigating the structural health of high-rise buildings and its influencing factors using Sentinel-1 synthetic aperture radar imagery: a case Study of the Guangzhou–Foshan metropolitan area. *Buildings* 14, 4074. doi:10.3390/buildings14124074

Karami, E., Alizadeh, N., Farhadi, H., Abdolazimi, H., and Maghsoudi, Y. (2023). Monitoring of land surface displacement based on SBAS-InSAR time-series and GIS techniques: a case study over the Shiraz Metropolis, Iran. *ISPRS Ann. Photogramm. Remote Sens. Spat. Inf. Sci.* 2022, 371–378. doi:10.5194/isprs-annals-X-4-W1-2022-371-2023

Magnússon, E., Björnsson, H., Rott, H., Roberts, M. J., Pálsson, F., Guđmundsson, S., et al. (2011). Localized uplift of Vatnajökull, Iceland: subglacial water accumulation deduced from InSAR and GPS observations. *J. Glaciol.* 57, 475–484. doi:10.3189/002214311796905703

Manunta, M., De Luca, C., Zinno, I., Casu, F., Manzo, M., Bonano, M., et al. (2019). The parallel SBAS approach for Sentinel-1 interferometric wide swath deformation time-series generation: algorithm description and products quality assessment. *IEEE Trans. Geosci. Remote Sens.* 57, 6259–6281. doi:10.1109/TGRS.2019.2904912

Martinelli, G., Chahoud, A., Dadomo, A., and Fava, A. (2014). Isotopic features of Emilia-Romagna region (North Italy) groundwaters: environmental and climatological implications. *J. Hydrol.* 519, 1928–1938. doi:10.1016/j.jhydrol.2014.09.077

Motagh, M., Djamour, Y., Walter, T. R., Wetzel, H.-U., Zschau, J., and Arabi, S. (2007). Land subsidence in Mashhad Valley, northeast Iran: results from InSAR, levelling and GPS. *Geophys. J. Int.* 168, 518–526. doi:10.1111/j.1365-246X.2006.03246.x

Ng, A. H.-M., Liu, Z., Du, Z., Huang, H., Wang, H., and Ge, L. (2023). A novel framework for combining polarimetric Sentinel-1 InSAR time series in subsidence monitoring—A case study of Sydney. *Remote Sens. Environ.* 295, 113694. doi:10.1016/j.rse.2023.113694

Picotti, V., and Pazzaglia, F. J. (2008). A new active tectonic model for the construction of the Northern Apennines mountain front near Bologna (Italy). *J. Geophys. Res. Solid Earth* 113. doi:10.1029/2007jb005307

Qiu, D., Wang, Y., Zhang, Y., Tong, Y., Liang, H., Ding, K., et al. (2023). Settlement monitoring data fusion approach for high-speed railways based on GNSS and InSAR. *J. Appl. Remote Sens.* 17, 034507. doi:10.1117/1.JRS.17.034507

Rizzo, A., Mattei, G., Dumon Steenssens, L., Anzidei, M., Aucelli, P. P. C., Alberti, T., et al. (2025). Methodological advances in sea level rise vulnerability assessment: implications for sustainable coastal management in a climate change scenario. *Ocean Coast. Manag.* 268, 107751. doi:10.1016/j.ocecoaman.2025.107751

Roque, D., Nuno Lima, J., Perissin, D., Paula Falcão, A., Lemos, J. V., and Fonseca, A. M. (2021). Integrated InSAR and GNSS monitoring subsystem for an arch dam and Reservoir banks. *J. Surv. Eng.* 147, 3. doi:10.1061/(ASCE)SU.1943-5428.0000361

Simeoni, U., and Corbau, C. (2009). A review of the Delta Po evolution (Italy) related to climatic changes and human impacts. *Geomorphology* 107, 64–71. doi:10.1016/j.geomorph.2008.11.004

Sala Calero, J., Vöge, M., Esteves Martins, J., Raucoules, D., de Michelle, M., et al. (2024). *EGMS validation report 2018-2022 update*. Available online at: https://land.copernicus.eu/en/technical-library/validation-report-2018-2022-dataset/@@download/file (Accessed January 29, 2026).

Sala Calero, J., Vöge, M., Esteves Martins, J., Raucoules, D., de Michelle, M., et al. (2023). *EGMS validation report*. Available online at: https://land.copernicus.eu/en/technical-library/validation-report-2015-2021-dataset/@@download/file (Accessed January 29, 2026).

Tapete, D., Morelli, S., Fanti, R., and Casagli, N. (2015). Localising deformation along the elevation of linear structures: an experiment with space-borne InSAR and RTK GPS on the Roman Aqueducts in Rome, Italy. *Appl. Geogr.* 58, 65–83. doi:10.1016/j.apgeog.2015.01.009

Teatini, P., Tosi, L., and Strozzi, T. (2011). Quantitative evidence that compaction of Holocene sediments drives the present land subsidence of the Po Delta, Italy. *J. Geophys. Res.* 116, B08407. doi:10.1029/2010jb008122

Tosi, L., Da Lio, C., Strozzi, T., and Teatini, P. (2016). Combining L-and X-band SAR interferometry to assess ground displacements in heterogeneous coastal environments: the Po River Delta and Venice Lagoon, Italy. *Remote Sens.* 8, 308. doi:10.3390/rs8040308

Veneto Region (2020). *WebGIS dei dati sentinel 1 – PS*. Available online at: https://idt2.regione.veneto.it/portfolio/webgis-dei-dati-sentinel-1-ps/ (Accessed September 10, 2025).

Wang, Q., Gao, Y., Gong, T., Liu, T., Sui, Z., Fan, J., et al. (2023). Dam surface deformation monitoring and analysis based on PS-InSAR technology: a case Study of Xiaolangdi Reservoir Dam in China. *Water* 15, 3298. doi:10.3390/w15183298

Wilkinson, M. W., McCaffrey, K. J. W., Jones, R. R., Roberts, G. P., Holdsworth, R. E., Gregory, L. C., et al. (2017). Near-field fault slip of the 2016 Vettore Mw 6.6 earthquake (central Italy) measured using low-cost GNSS. *Sci. Rep.* 7, 4612. doi:10.1038/s41598-017-04917-w

Xiao, R., Gao, X., Wang, X., Yuan, S., Wu, Z., and He, X. (2024). Measuring dam deformation of long-distance water transfer using multi-temporal synthetic aperture radar interferometry: a case study in south-to-north water diversion project, China. *Remote Sens.* 16, 365. doi:10.3390/rs16020365

Yaragunda, V. R., and Oikonomou, E. (2024). "Monitoring the los (line of sight) deformation of the corinth canal, Greece using SBAS and GNSS techniques," in *Proceedings of the IEEE international geoscience and remote sensing symposium (IGARSS 2024)*. Athens, Greece, 11056–11061. doi:10.1109/IGARSS53475.2024.10642704

Yeh, T.-K., Lee, T.-Y., Lee, I.-H., Shih, H.-C., Chen, C.-H., Yen, J.-Y., et al. (2025). Combination on GNSS precise point positioning and InSAR data fusion to monitor the land subsidence in Taiwan. *Geomat. Nat. Hazards Risk* 16, 2445632. doi:10.1080/19475705.2024.2445632

Yuwono, B. D., and Prasetyo, Y. (2018). Analysis deformation monitoring techniques using GNSS Survey and terrestrial Survey (case study: diponegoro university dam, semarang, Indonesia). *IOP Conf. Ser. Earth Environ. Sci.* 313, 012045. doi:10.1088/1755-1315/313/1/012045

Zhu, M., Liu, H., Miao, C., Li, G., Zhang, Y., Zhou, Y., et al. (2025). Safety assessment of the Qinghai–Tibet railway: monitoring, analysis, and prediction. *Cold Reg. Sci. Technol.* 231, 104395. doi:10.1016/j.coldregions.2024.104395